Earth and Planetary Science Letters 554 (2021) 116642

Contents lists available at ScienceDirect

Earth and Planetary Science Letters

www.elsevier.com/locate/epsl

Pervasive low-velocity layer atop the 410-km discontinuity beneath the northwest Pacific subduction zone: Implications for rheology and geodynamics

Guangjie Han [a,b,c], Juan Li [a,b,c,d,*], Guangrui Guo [a,b,c], Walter D. Mooney [e], Shun-ichiro Karato [f], David A. Yuen [g,h]

[a] Key Laboratory of Earth and Planetary Physics, Institute of Geology and Geophysics, Chinese Academy of Sciences, Beijing 100029, China
[b] Innovation Academy for Earth Science, Chinese Academy of Sciences, Beijing 100029, China
[c] College of Earth and Planetary Sciences, University of Chinese Academy of Sciences, Beijing 100049, China
[d] Mohe Observatory of Geophysics, Institute of Geology and Geophysics, Chinese Academy of Sciences, Beijing 100029, China
[e] United States Geological Survey, MS 977, 345 Middlefield Road, Menlo Park, CA 94025, USA
[f] Department of Earth and Planetary Sciences, Yale University, New Haven, CT 06520, USA
[g] Department of Applied Physics and Applied Mathematics, Columbia University, New York, NY 10027, USA
[h] Department of Computer Science and Geosciences, Ocean University of China, Qingdao 266003, Shandong, China

ARTICLE INFO

Article history:
Received 18 June 2020
Received in revised form 30 September 2020
Accepted 14 October 2020
Available online 6 November 2020
Editor: J. Brodholt

Keywords:
low velocity layer atop the 410
mantle transition zone
waveform modeling
wetting of grain boundary
Northwest Pacific subduction zone
water-bearing MTZ

ABSTRACT

Regional triplication waveforms of five intermediate-depth events are modeled to simultaneously obtain the compressional (P) and shear (SH) wave velocity structure beneath northwestern Pacific subduction zone. Both the P- and SH-wave velocity models for three different sub-regions show a low-velocity layer (LVL) with a thickness of ∼55-80 km lying above the 410-km discontinuity with a ∼900 km lateral extent from the Japan Sea to the northeastern Asian continental margin. With the dihedral angle approaching to zero around 400 km, a minute amount of melt atop the 410-km discontinuity caused by the hydrous slab might completely wet olivine grain boundaries and result in a low seismic velocity layer in this specific subduction zone. This mechanism suggests that the 410-LVL is a low viscosity zone that would partially decouple the upper mantle from the transition zone. We infer that the widespread 410-LVL provides evidence for a water-bearing mantle transition zone beneath the western Pacific subduction zone.

1. Introduction

The mantle transition zone (MTZ), a layer between the upper and lower mantle, plays a crucial role in mantle convection and dynamic processes. The upper and lower interfaces of the MTZ, the '410-' and '660-' km discontinuities (hereafter referred to as the 410 and the 660, respectively), are due to phase changes within the olivine rich upper mantle (e.g. Ito and Takahashi, 1989).

The 410 is marked by a distinct velocity increase and has been reported to be overlain by a low velocity layer. However, the global distribution, seismic and physical characteristics, and mechanism of formation of the low velocity layer above the 410 (410-LVL hereafter) has been debated for years. An early investigation was reported by Revenaugh and Sipkin (1994), in which they studied long period multiple-ScS reverberations and imaged a ∼5.8% impedance decrease at a depth of around 330 km beneath easternmost Asia, Sea of Japan and Yellow Sea. Since then, the presence of 410-LVL has been observed sporadically in some regions, such as subduction zones (Tauzin et al., 2017), ancient continental platforms (Vinnik, 2002), or nearly globally (Tauzin et al., 2010). The 410-LVL can be identified using different seismic phases, most importantly PS and SP converted waves (also referred to as P and S receiver functions), body wave triplications, SS precursors and ScS reverberations, with the estimated thickness ranging from 20 to 90 km (e.g. Jasbinsek and Dueker, 2007; Bagley et al., 2009; Wei and Shearer, 2017).

In addition to being the first study area of the 410-LVL, the northwest Pacific subduction zone is an ideal location to investigate the interaction between the subducting slab and the MTZ, as manifested by variations in the seismic structure around the mantle discontinuities (Fig. 1). The slab is imaged to be lying sub-

* Corresponding author.
E-mail address: juanli@mail.iggcas.ac.cn (J. Li).

https://doi.org/10.1016/j.epsl.2020.116642
0012-821X/

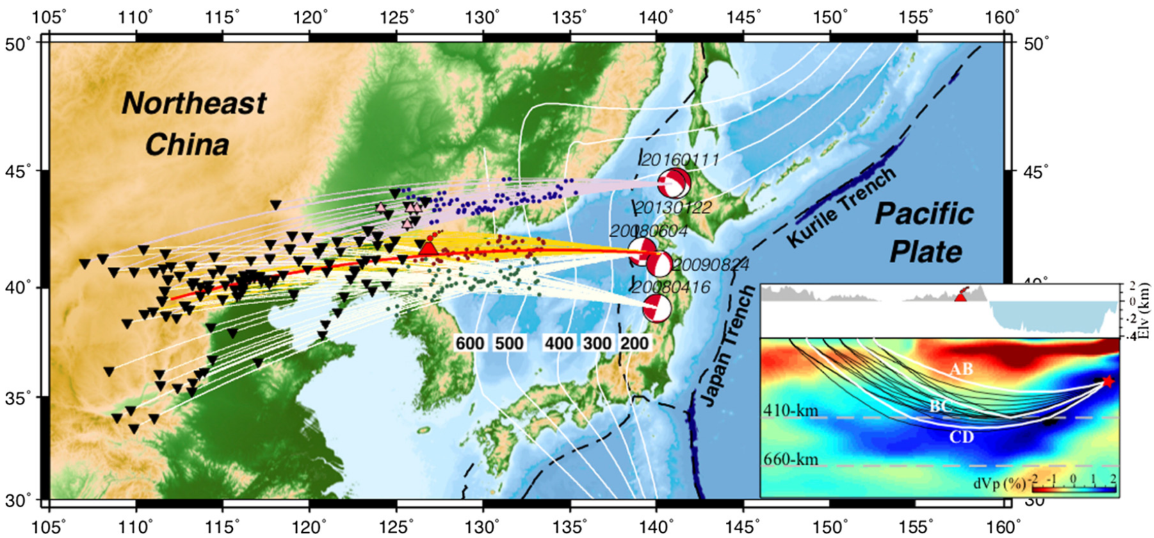

Fig. 1. Location map of intermediate-depth events and dense regional seismic stations used in this study. Focal mechanisms for the five events used in triplication waveform modeling are shown with red beach balls. Permanent seismic stations are shown by black inverted triangles, and the temporary NECsaids array seismic stations are represented by pink solid triangle. The red triangle denotes the Changbaishan volcano. The purple, yellow and white lines represent rays traveling below the 410 for northern events (20130122 and 20160111), middle events (20080604 and 20090824) and southern events (20080416 and 20080604). Dark blue, red and green series dots are turning locations of CD phases calculated for the Iasp91 model. The lower-right inset shows ray paths along the red profile west of the northern Honshu arc with the P velocity from GAP_P4 as the background (Fukao and Obayashi, 2013). The color scale for the velocity perturbation is $\pm 2\%$. The gray dashed lines in the inset indicate the top (410 km) and the lower boundary of the transition zone(660 km). The black lines represent raypaths of the triplicated waves calculated via Tau-P using the Iasp91 model, and the white lines indicate the raypaths of AB, BC and CD phases. (For interpretation of the colors in the figure(s), the reader is referred to the web version of this article.)

horizontally within the MTZ with a ~1500 km westward extension (Fukao and Obayashi, 2013). A low-velocity big mantle wedge exists above the stagnated slab (Zhao and Ohtani, 2009). Corner flow in the big mantle wedge and the dehydration of the deep slab in the MTZ are proposed to account for asthenospheric upwelling and intraplate volcanism in eastern China (Zhao and Ohtani, 2009). Finite frequency tomography images show a slab "gap" in the stagnant Pacific slab above the 660, through which the subduction-induced upwelling escapes and produces decompression melting to feed Changbaishan volcano and neighboring volcanoes (Tang et al., 2014). However, tomographic modeling has a limited ability to constrain the detailed structure of the MTZ due to the intrinsic problems of damping-associated inversion techniques and poor resolution at depth. These limitations are especially true for seismic models of the 410-LVL which are critical for the discrimination of models for regional scales of convection and the mechanisms of the intraplate volcanoes.

Body wave caustic waveform modeling is an effective method for constraining the seismic velocity structure of mantle discontinuities (Ye et al., 2011; Li et al., 2013; Wang et al., 2014). In contrast to receiver function analysis, waveform modeling provides information on both velocity variations and depths of interfaces when the geometry of dense seismic stations and source is optimal (Li et al., 2016a). In this study, our goal is to determine the detailed velocity structure around the 410-km discontinuity. We applied regional waveform modeling to high-quality broadband seismic data recorded by the Chinese Regional Seismic Network and a temporary seismic array to obtain P and SH velocity models for the 410-LVL. Our study covers a "gap and blank" region located across the western part of the Japan sea and the Northeast Asian continent. We discuss the robustness of the 410-LVL model and its possible origin. We propose that wetting of grain boundaries plays an important role in reducing seismic velocities in the cold subduction zone. Finally, we discuss the rheological and dynamical implication of a pervasive 410-LVL in a context of the subducting system in East Asia.

2. Method and data

When seismic waves encounter a sharp velocity discontinuity or a thin layer with a high velocity gradient, the ray paths will bend and produce caustic waveforms, also called triplicated phases. Fig. 2a illustrates the wave turning above the discontinuity (AB), the wide-angle reflection off the discontinuity (BC) and the wave diving below the discontinuity (CD). Because the pathways of triplicated phases lie very close to each other in the shallow earth, differences in the relative time interval and amplitude between different branches, and especially the location of the caustic points are highly sensitive to the velocity structure near the discontinuity (Fig. 2a). Taking the 410 as an example, the travel time difference between the phases AB and CD mainly reflects the velocity contrast above and below the 410. When a LVL with anomaly of -1.5% and thickness of 70 km lies just above the 410, the termination distance of phase AB (i.e. the location of cusp-B) will appear at the larger distance of ~21.4° (~18.3° for the Iasp91 model). For an earthquake with intermediate-depth of 220 km, the crossover point O of phases AB and CD (the location of cusp-O) will increase ~0.6°, and the travel-time difference between the two phases will be much larger (Fig. 2b). A densely-recorded seismic wavefield at the appropriate distance range is important to capture the entire set of caustic waveforms and thus to resolve the seismic structure details (e.g. Li et al., 2013).

2.1. Seismic data pre-processing

We mainly use seismic records from the permanent China Digital Seismograph Network (CDSN; Zheng et al., 2010), and we have carefully selected five events that occurred in Japan Sea between the years 2008 and 2016. To avoid effects due to the complexities of shallow structure, the depths of these events were restricted to between 150 and 300 km (Table 1). In addition, for two of these events we gathered the waveforms of four stations from a temporary broadband seismic array, NECsaids (NorthEast China Seismic Array to Investigate Deep Subduction; Wang et al., 2016), which recorded data intermittently from 2011 to 2016 (Fig. 1). All events display simple source time functions (STFs), and those recordings

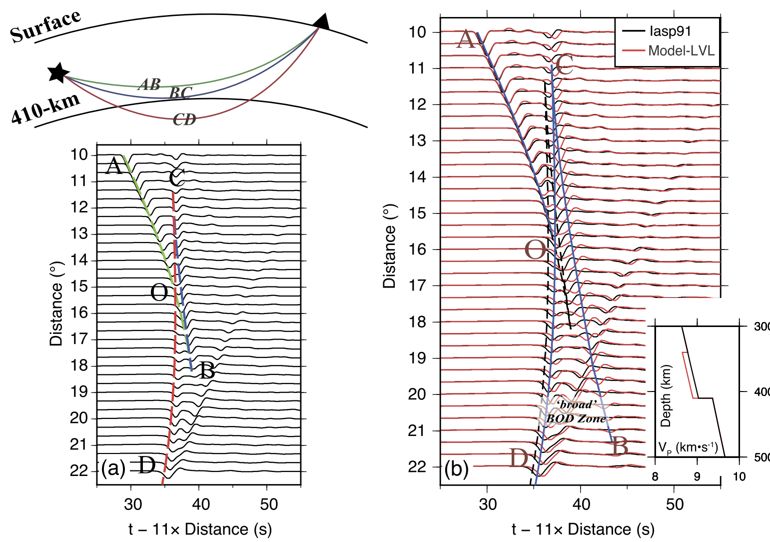

Fig. 2. Diagrams of ray-paths of caustic waveforms and synthetic seismograms for two velocity models. The synthetics are made for event 20080604, and the hypocentral parameters are shown in Table 1. (a) The 3 branches of the triplicated phases AB phase (green solid line), BC phase (blue solid line) and the CD phase (red solid line). Theoretical vertical waveforms are calculated from Iasp91 model, with green, blue and red dashed lines representing travel times of the AB, BC and CD phases. (b) Comparison of synthetic waveforms calculated from Iasp91 and a model with a low velocity anomaly of −1.5% with thickness 70 km atop the 410. The black dashed and blue solid lines show the travel time curves; black and red lines are synthetic waveforms corresponding to the Iasp91 model and Model-LVL, respectively. The cusp-B, and -C indicate the termination distance of phase AB and the appearance of phase CD, respectively; the regions between AB and CD phases cut-crossed by the cusp-O are regarded as zones AOC and BOD, and a 'broad BOD' means an obvious larger travel time differences between AB and CD phases.

Table 1
Information of events used in triplication waveform modeling.

Event ID	Origin time		Location		Mag. (Mw)	Depth (km)		Duration time (s)	
			Lat (°)	Lon (°)		PDE	CMT/Relocated	Z	T
20080416	16/04/2008	19:19:38.5	39.08	140.18	5.8	166	169	4	–
20080604	04/06/2008	17:03:08.0	41.50	139.15	5.7	205	204/220*	3.5	4
20090824	24/08/2009	05:26:17.4	41.50	140.18	5.3	176	171	3	–
20130122	22/01/2013	13:29:25.6	44.45	140.83	5.4	235	248	3	–
20160111	11/01/2016	17:08:06.5	44.46	140.01	6.3	239	254	3	–

Z: Vertical component.
T: Transversal component.
-: This component hasn't been used in the study due to low SNR.
*: The CMT depth of event 20080604 is 204 km, and we relocated it as 220 km, which is used in all the synthetic waveform calculations. Depth for the other events are from CMT.

with a signal-to-noise ratio (SNR) greater than 6 on the vertical component were selected from a total of 177 stations. Waveforms for both P and S triplication were selected for analysis. The ray paths cover a region within 124-134°E and 38-45°N. Li et al. (2013) investigated the detailed P and SH-wave velocity structure in the deep MTZ beneath this region, providing us an opportunity to account for the effects of the 660 and focus on the seismic structure around the 410.

Triplication waveforms might be distorted by the complex 3D structure in subduction region. Wang et al. (2014) conducted a series of synthetic tests for a model with a flat slab trapped in the MTZ, and concluded that when ray paths are perpendicular to the strike of the slab, the 1D waveforms are a good approximation to the synthetic waveforms generated by a 3D model. Therefore, we confined our study to a fan-shaped region defined by the ray paths roughly perpendicular to the strike of the Wadati-Benioff zone. To further reduce the effects of lateral velocity variations, we confined the distribution of stations to a narrow azimuthal range for each event, with an average azimuthal range of ∼9° (Fig. 1). Finally, we divided these five events into three groups according to the sampling points: the northern region (events 20130122 and 20160111), the middle region (events 20080604 and 20090824), and the southern region (events 20080604 and 20080416), respectively. The records of the four stations of the temporary NECSaids array are available for events 20160111 and 20130122. We noted that using two independent events in one region provides redundancy that helps verify the velocity structure. The turning points of the CD phase sample a broad region beneath Japan sea and the border of China (Fig. 1) with a lateral range of ∼900 km, and a north-south extent of ∼500 km. For those events with clear SH-wave triplications, we use a nearly same station-event geometries for both P- and SH-waves.

Several steps are involved in our data pre-processing. First, we removed the instrumental responses from all records. We then applied a Butterworth bandpass filter with frequency band 0.04-1.0 Hz and 0.04-0.5 Hz to the vertical and transverse component seismograms, respectively (Li et al., 2013). We inspected both horizontal components to verify the correct polarities of signals (Niu and Li, 2011; Wang et al., 2016). Second, we recalculated the source depth of the events. For event 20080604, we relocated the event at a depth of 220 km using teleseismic data available from the Incorporated Research Institutions for Seismology (IRIS). This depth is 10 km deeper than the depth reported in the ISC catalogue. Because the SNR in the teleseismic waveforms for the other four events are lower, we adopted the hypocentral depth from the Global CMT (Table 1). It should be noted that the uncertainty of hypocentral depth has little influence on relative travel times and amplitudes of the triplicated phases, which are the critical factors in the waveform modeling. For example, a 10 km uncertainty in the focal depth will only result in a difference of ∼ 0.1 s in the travel time difference between the AB and CD phases. For the generation of synthetic seismogram, we applied the reflectivity method developed by Wang (1999). The source mechanisms are from the Global CMT catalog, and a Gaussian wavelet is used to represent the source time function, with the source duration time listed in Table 1.

In the aligned records of vertical and transverse components of all events, we observed a ubiquitous delay of the P and S arrivals even at shorter epicentral distance relative to the Iasp91 reference model. To compensate the large P and S time residuals, we adopted a similar approach as Li et al. (2013) by adding a low velocity layer at a shallow depth of ∼165 km, which greatly improved the consistency in P and S absolute travel times. After making this correction, the velocity structure around the 410 are further constrained by triplication waveform modeling.

2.2. Grid search process

Each branch of the triplication constrains a specific part of the target seismic velocity structure (Fig. 2b). We emphasized two aspects of the data to constrain the best fitting models. The first key aspect of the data is the location of cusp-B. We calculated the residuals of the termination distance of the AB phase between the synthetics and the observed values with ray tracing. The second key aspect of the data is the variation of waveforms, especially the change of the travel time difference between the AB and CD phases. We focused on the waveform features related to the 410, and calculated the correlation coefficients between the synthetic and observed triplications in a variable time window to effectively minimize the influence of noise. It should be noted that in order to avoid distortions of the waveforms due to the effects of triplication branches generated by the 660-km discontinuity, we mainly focused on the waveforms with distance smaller than ∼19° corresponding to a ray turning depth of ∼470 km.

We applied the two aspects of the data mentioned above to determine a pair of key features in the velocity structure around the 410: (1) the magnitude of the velocity reduction of the LVL, (2) the depths of upper and lower interfaces of the 410-LVL. The velocity reduction can be varied from 0-4% with respect to the Iasp91 model, and the depth of the lower and upper interfaces of the 410-LVL is allowed to vary between 360-420 km and 310-360 km respectively, considering a subduction background; We then explored the whole parameter space, and looked for the maximum correlation coefficient value within a range of the minimum residual value for the location of cusp-B (Supplementary Material S1.1). We assessed the agreement between the theoretical and observed seismograms, and select the model with the highest correlation co-

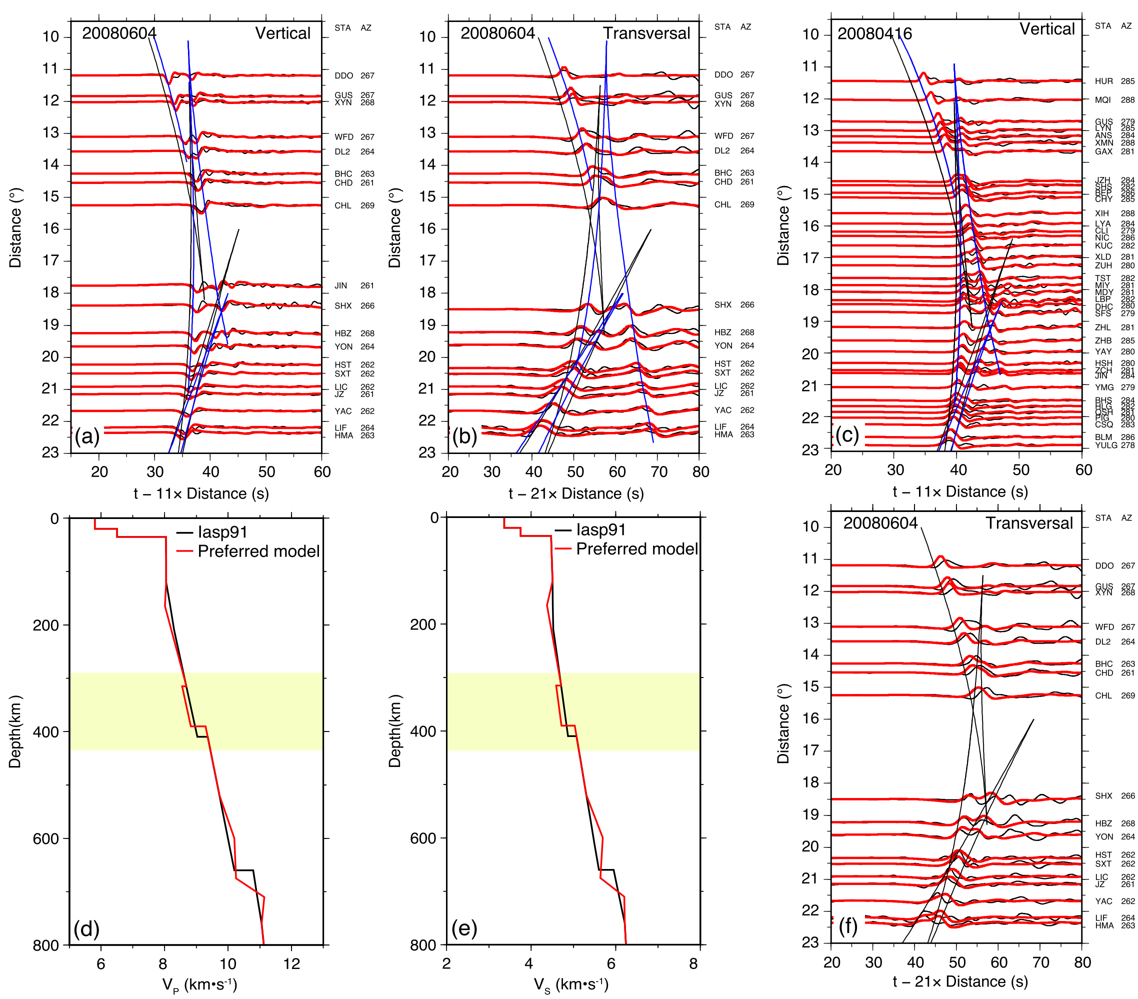

Fig. 3. Comparison of the observed (black solid line) and synthetic (red solid line) vertical and transverse displacement waveforms for the southern region for the two events used (20080604 (a, b) and 20080416 (c)). Black lines and blue lines are theoretical travel times based on the Iasp91 and preferred models, respectively. (d, e) Preferred velocity models (red lines), and the yellow regions highlighting the location of the LVL. The black line marks the reference model Iasp91 for comparison. The transverse component of synthetic seismogram based on Iasp91 for event 20080604 is plotted in (f). The long extension of cusp-B and the enlarged time difference between AB and CD phases at distances larger than 18.5° cannot be matched.

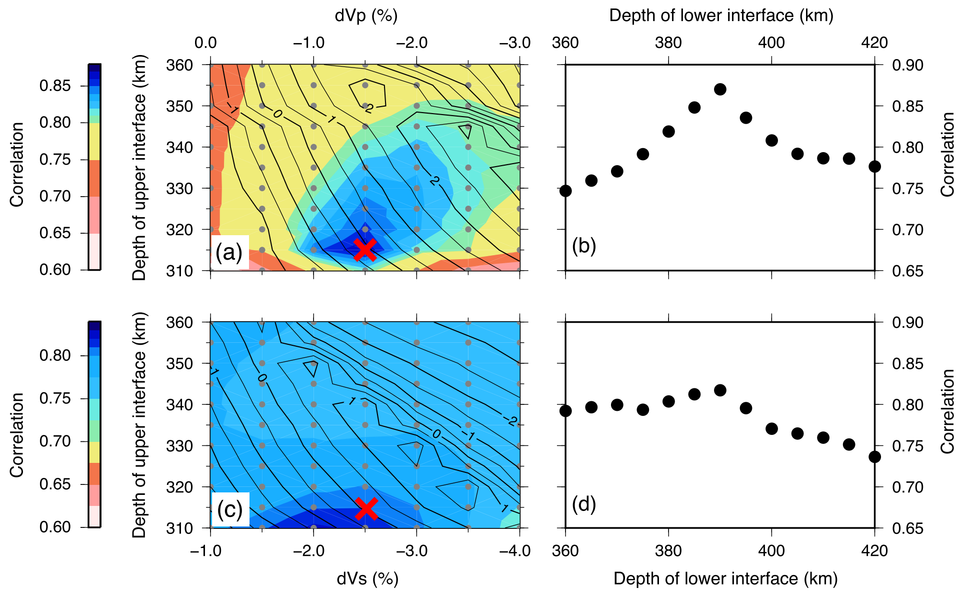

Fig. 4. Grid search process for detecting the best fitting models of southern region as determined by the correlation coefficient and location of cusp-B. In the left column (a, c), gray circles are the grid points. The contour map shows the correlation coefficients calculated for a grid with varied depth of the upper interface and the velocity anomaly across the 410. The lines are the contours of the residual of the cusp-B. The red crosses represent the best fitting models. The right column shows the correlation coefficient calculated for the lower interface of the 410-LVL.

efficient as the best fitting model. In the grid search process, the depth step is 5 km and the velocity step is −0.5%.

3. Data analysis and triplication waveform modeling

3.1. Southern region

The southern region is roughly confined within the area between 39.5°N and 41.5 °N. In the aligned vertical and transverse waveforms of events 20080416 and 20080604, we can see obvious triplicated phases for the 410 at regional distances of 10-23°. Taking event 20080604 as an example, the vertical waveforms show the following characteristics: the AB phase becomes indiscernible at a distance greater than ∼19.6°; the most obvious feature is the travel time difference between the AB and CD phases, which is much larger than the value predicted from the Iasp91 model (Fig. 3a). The transverse component waveforms, with lower SNR, show similar features in the aligned seismogram: the AB phase extends to as far as ∼22.7°. In particular, we observed an obvious broadened BOD zone with significantly delayed AB phase (Fig. 3b), which is impossible to fit by using the Iasp91 model (Fig. 3f). The vertical component waveforms of event 20080416 share similar features to event 20080604 (Fig. 3c), however, the SNR in the transverse component of this event is rather low, and no triplication can be clearly identified. The commonality of the key features in the seismic triplication waveforms for these two events imply that they are robust observations of the 410-LVL structure under this region.

It should be noted that triplication caused by the 660 is also observed clearly in the waveforms at larger distances (> ∼19°). When the structure of the lower part of the MTZ is taken from the Iasp91 reference model, some major discrepancies between observed and synthetic waveforms apparently. Some previous researchers used triplication waveforms to model the detailed P and SH structure around the 660 beneath the study area and adjacent regions (e.g. Wang et al., 2006; Ye et al., 2011; Li et al., 2013). Considering the distribution of data, lateral variations of the MTZ, and the subtle effects of variations in physical properties on the P and S velocities, we thus referred to the model of Li et al. (2013) around the 660 to account for the effect of "flat" slab (the slice of slab image in Fig. 1), which significantly improved the agreement between the synthetic seismograms and observed records.

Through a thorough grid search in the parameters space (Fig. 4), we obtained the best fitting compressional and shear velocity models (hereafter referred to as the P and SH models, respectively). Both models show that a LVL with a thickness of 75 ± 15 km lying above the 410, and the seismic velocity anomalies are −1.5 ± 0.4% and −2.5 ± 0.6% for P- and SH-waves respectively (Fig. 3d, e). Uncertainty estimation is presented in Supplementary Materials S2.

3.2. Middle region

Two events (20080604 and 20090824) are used to detect the detailed structure around the 410 beneath the middle region. For the vertical component of event 20090824, the observed AB branch extends to as far as ∼20.6°, much further than the predicted distance of 19.2° as calculated from the Iasp91 model; an obvious 'broad' BOD zone with delayed AB phase appears after a distance of ∼16.5° (Fig. 5c). The second event shares similar features as the first one. In Fig. 5d and e, we show our preferred models for the middle region.

A LVL above the 410 is required to account for the striking characteristic of the long extension of the AB phase and the 'broad' BOD zone. The strength of the 410-LVL is −1.5 ± 0.4% and −2.5 ± 0.6% with thickness 80 ± 19 km (Fig. 5d, e) for the best fitting P and SH models, respectively.

3.3. Northern region

We have good evidence for the existence of the 410-LVL in the northern region. The long extension of the cusp-B and a clear 'broad' BOD zone are observed in the aligned vertical seismograms for both events (20130122 and 20160111), which verifies that the 410-LVL is an intrinsic feature of the deep structure (Fig. 5f, g). The transverse components for both events have relative low SNR and seem to show some distorted features related to the local slab structure, which will be left for further detailed investigations. Consistent with the other two regions, our preferred P model

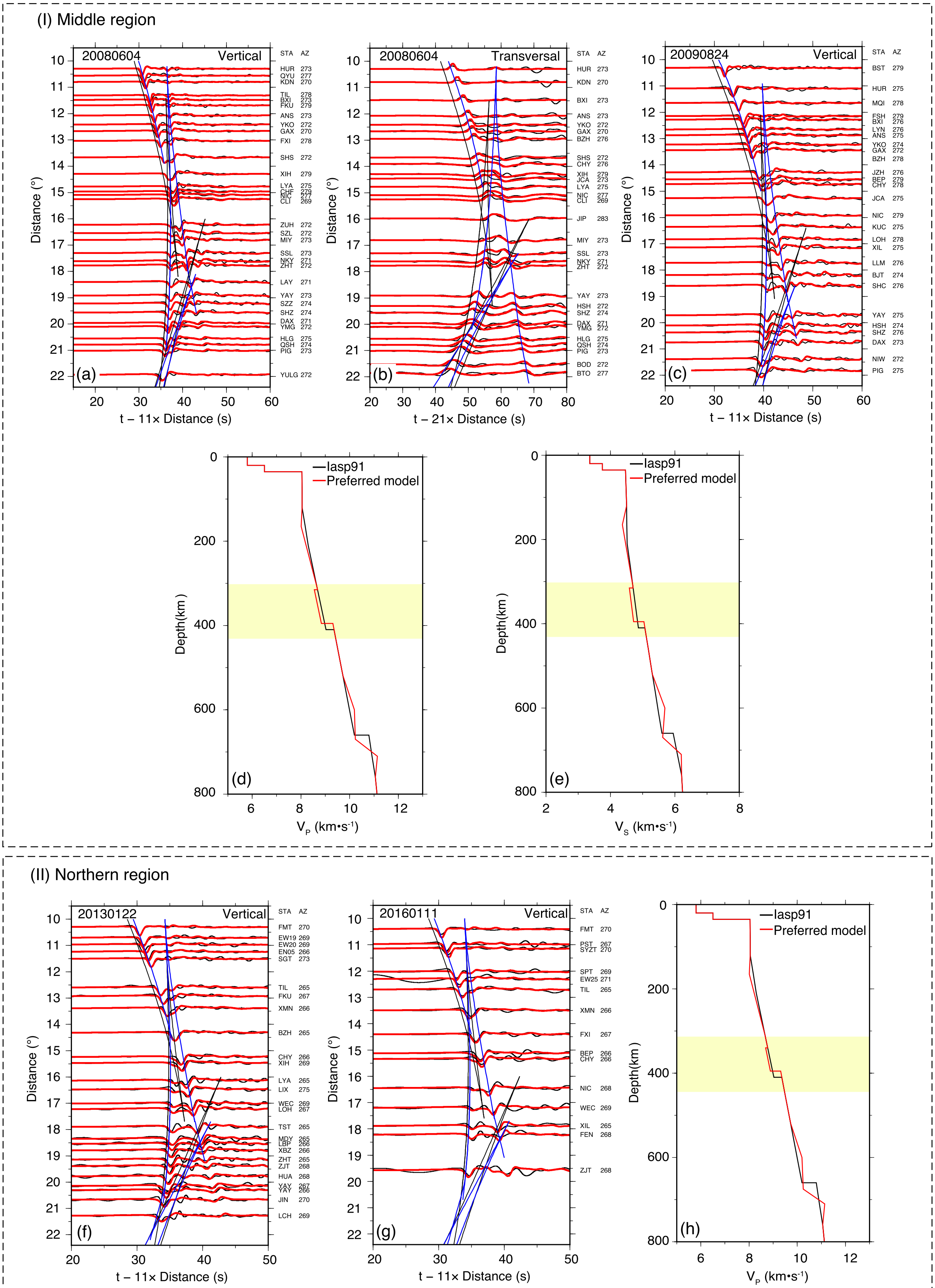

Fig. 5. Comparison of the observed (black solid lines) and synthetic (red solid lines) vertical and transverse displacement waveforms for the middle (a, b, c) and northern regions (f, g). Black lines and blue lines are theoretical travel times based on Iasp91 and the preferred model calculated from Tau-P, respectively. (d, e) and (h) are preferred velocity models (red solid lines) around the 410-km discontinuity for the middle and northern regions. The black solid line marks the reference velocity model Iasp91 for comparison.

shows a low velocity anomaly (-1.0 ± 0.5%) with thickness 55 ±17 km just atop the 410 (Fig. 5h).

3.4. An integrated view

We have determined P- and SH-wave velocity models beneath the northwest Pacific subduction zone, and several consistent features are observed in these models. The most important feature is the existence of a low velocity layer just above the 410 with thickness varying from 55 to 80 km. From the distribution of reflection points of the CD phase, we can constrain the 410-LVL to be located beneath the northwest Japan Sea and northeast China (124-134°E, 38-45°N). Moreover, it covers a region with a roughly east-west lateral range of nearly 900 km. It should be noted that, in each of the three sub-regions studied, we used two independent events to constrain the velocity structure around the 410, thereby confirming the consistency of the observed features and robustness of our P and SH velocity models.

We have carried out a quantitative analysis to verify the robustness of the 410-LVL structure derived here. We calculated the correlation coefficient of the observed and synthetic waveforms predicted for the Iasp91 model and our best fitting models, respectively (cross correlations available in Supplementary Materials S1.2). For all regions, the correlation coefficients of the best fitting models are significantly higher than those predicted by the Iasp91 model. The consistency of these observations and the agreement among the best fitting models indicates that the 410-LVL structure is a robust feature.

4. Discussion and interpretation

We simultaneously obtained P- and SH-wave velocities near the top of the 410 in northwestern Pacific subduction zone through triplication waveform modeling of five intermediate-depth earthquakes. Several consistent features are observed in both the P and SH velocity models, and the most prominent one is the existence of 410-LVL with a P-wave velocity reduction of about 1.0-1.5%, SH-wave reduction of about 2.5%, and a thickness between 55-80 km, with the uncertainty estimate of 17 km.

4.1. The robustness of obtained models

Our models inferred a 55-80 km thick LVL above the 410 in the Pacific subduction zone. A trade-off exists between the amplitude of the velocity anomaly and the thickness of the 410-LVL. Considering event 20080604 which samples the middle region, the best-fitting P-wave velocity model shows a LVL with a 80 km thickness and a velocity reduction of ~1.5% (Fig. 5d). We can also use a model with 65 km thickness and −3% velocity anomaly to match the width of BOD. The location of cusp-B according to this alternative model, however, is extended to 21.4°, much further than the observed distance of ~19.6° (Fig. 5a). Thus, the thickness and the

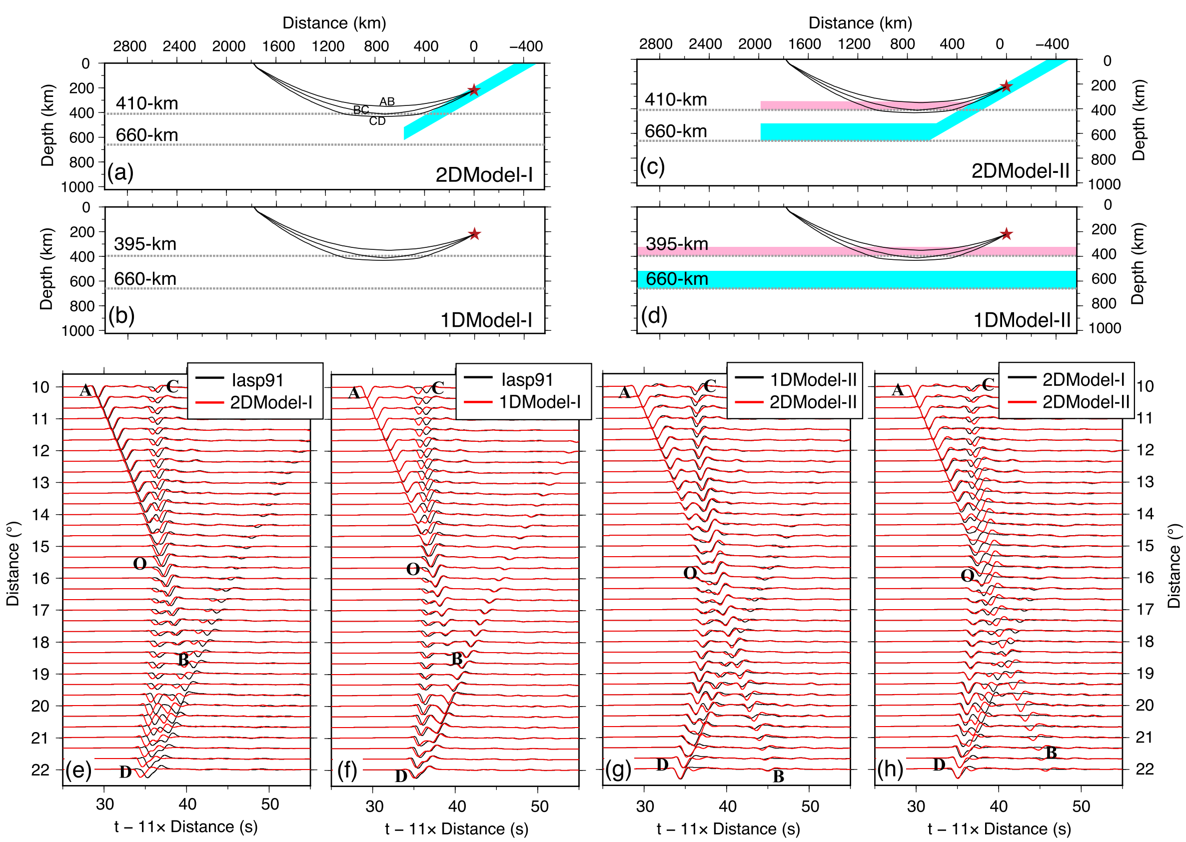

Fig. 6. Synthetic waveform comparisons between different 1D and 2D models. The source is placed at a depth of 220 km and 23 km from the upper interface of the slab. All the models are based on the Iasp91 model. (a) 2DModel-I: a dipping portion of the slab with a dip angle of 30° is added, and the P-wave velocity anomaly is set to be 1.5%. (b) 1DModel-I: the 410 is set to be 15-km-uplifted and no slab is considered. (c, d) 2DModel-II and 1DModel-II: the stagnant portion of the slab with thickness ~140 km and the 410-LVL with P-wave velocity reduction of 1.5% are included based on previous two models. The epicenter distance for the illustrated three raypaths (black lines) is 16°. (e) Synthetics for Iasp91 model (black lines) and 2DModel-I (red lines), with the cusp points marked for the red synthetic curves. The CD phase appears earlier showing the influence from the ray traveling in the slab with high velocity. (f) Synthetics for Iasp91 (black lines) model and 1DModel-I (red lines). A similar and comparable feature to that of the model 2DModel-I, especially at distance smaller than 20°, indicates the influences on the waveforms caused by the dipping portion of slab can be partly compensated by the uplift of the 410. (g) Synthetics for 1DModel-II (black lines) and 2DModel-II (red lines). Expect tiny differences of the amplitudes, the synthetic waveforms of two models show similar features in the location of cusp-B and the width of BOD zone. (h) Synthetics for 2DModel-I (black lines) and 2DModel-II (red lines). The long extension of cusp-B and the widening BOD zone show the influences from the 410-LVL.

velocity anomaly of the LVL are well constrained by careful modeling of different specific aspects of the triplication.

In our study region, seismic tomography images have revealed a prominent subducting slab (e.g. Fukao and Obayashi, 2013; Ma et al., 2018) that is stagnant atop the 660 for more than 1500 km. To address the effects of the slab on the detection of the 410-LVL, we conducted series of 2D waveform modeling tests. A finite difference scheme is applied in the calculation of seismograms (Li et al., 2014). First, we explored the influences on the waveform caused by the dipping portion of the slab (Fig. 6, 2DModel-I). The ray of the CD phase travels in the slab with high velocity, resulting in an earlier appearance of the phase and a widened of the BOD zone (e.g. ~0.3 s in the distance range of 16-18°, Fig. 6e). However, the cusp-B shows no extension. Meanwhile, we compared another model with an elevated 410-km discontinuity (1DModel-I). A similar and comparable feature to 2DModel-I could be detected (Fig. 6f), which indicates that the elevation of the 410 can compensate the variation of the waveform caused by the dipping portion of the slab. Thus it is evident that with an appropriate 1D station-event geometry, e.g. one with a limited azimuthal range and raypaths perpendicular to the strike of the slab, we can extract the details related with the 410-LVL, even for such a complicated subduction system.

We then took the stagnant portion of the slab and the 410-LVL into consideration (2DModel-II and 1DModel-II) on the basis of previously published models. Despite small differences in the amplitude of the triplicated phases, both synthetic waveforms show similar features in the location of cusps-B and -C, and in the width of BOD zone (Fig. 6g). The influence on the 410 triplicated phases caused by the stagnant portion of the slab are almost the same for 2DModel-II and 1DModel-II and is due to the presence of the high velocity layer atop the 660 in both models. Hence, these results confirm that the effects on the waveforms due to the 15-km-uplift of the 410 is analogous to that of the dipping slab. One major feature of the long extension of the cusp-B to ~21°, however, can be clearly identified, and this is caused by the LVL above the 410. The distinct features of the long extension of cusp-B and the broadened BOD zone due to the 410-LVL are compared and is illustrated in Fig. 6h and Fig. S5, which can be regarded as a resolvable fingerprint of the low velocity layer. More detailed information can be found in Supplementary Material S3 & S4.

We have an elevated 410-km discontinuity with a depth that varies between 390 and 395 km beneath the three regions. However, investigations on the topography of the mantle discontinuities from receiver function analysis and ScS multiple waves indicate that our study region is located in a marginal zone with an insignificant depth variation in the 410 (e.g. Tian et al., 2016; Wang et al., 2017). We thus argue that the 15-20 km uplift of the 410 in our models might be overestimated, and may compensate for the effects on the waveform caused by the dipping portion of the slab. The influences of the dipping portion of the slab can also explain some mismatches on the amplitude of phases BC and CD between the synthetic and observed waveforms, especially when the epicentral distance is smaller than 16° (Fig. 5b).

4.2. Comparison with previous 410-LVL investigations

Multiple methods have been applied to detect the velocity structure around the 410 beneath northwest Pacific subduction zone and the 410-LVL has been reported sporadically with variable resolution. Tauzin et al. (2017) applied P-S receiver function analysis to teleseismic waveforms recorded beneath the mainland of Northeast China, the Japan Islands and the Korean Peninsula. The seismic amplitudes provide an indication as the existence of negative SH-wave velocity zone atop the 410 in the following four zones: I. the Korean Peninsula and Kyushu; II. the Songliao sedimentary basin in northeast China; III. Hokkaido; and IV. Honshu (Fig. 7). The estimated shear wave velocity reduction in their results is about 2-4%. Because the CCP stacked amplitudes do not exceed the 68% confidence level in some regions, the 410-LVLs report by Tauzin et al. (2017) don't seem to be continuous. Our study region is mainly located in the gap between zones I and II of Tauzin et al. (2017), and the northern part is slightly overlapping with zone II. Significantly, our study region covers an important "gap and blank" region beneath the western part of the Japan Sea, where the distribution of seismic stations is limited, and the traditional receiver function technique cannot be applied.

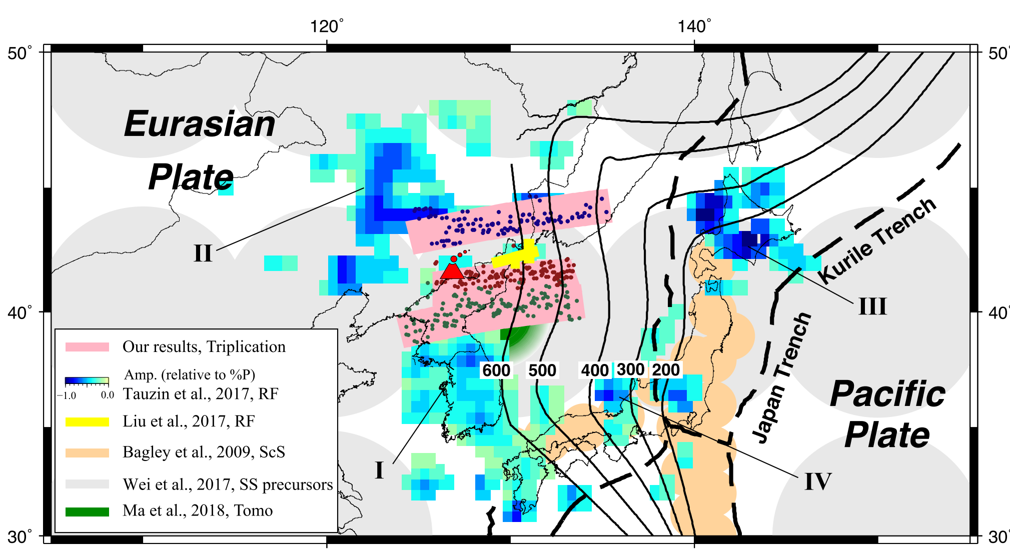

Fig. 7. Integrated map of the distribution of the 410-LVL detected in previous studies and our observations for the northwestern Pacific subduction zone. Squares represent amplitudes of seismic signals obtained by receiver function analysis (Tauzin et al., 2017); zones in blue indicate regions with obvious negative amplitudes, and the 410-LVL is observed in four major zones (labeled I, II, III, IV). The large gray circles represent results from SS precursor studies (Wei and Shearer, 2017), with an average lateral resolution of ~500-750 km. The orange circles show results of ScS multiple reverberations (Bagley et al., 2009). The yellow rectangles represent results given by Liu et al. (2016), using the receiver function technique. The green circle shows result from Ma et al. (2018), with about −1.5% P-wave velocity anomaly, by performing joint inversions of local and teleseismic events. The middle pink near-rectangle regions with dots in different colors show the distribution of 410-LVL in our study.

Liu et al. (2016) applied the receiver function technique to northeast China and observed the 410-LVL as indicated by high-negative amplitude pulses in the region east of Changbaishan volcano (128-132°E between 41°N and 43°N). Wei and Shearer (2017) used long-period SS precursors and detected sporadically distributed 410-LVLs worldwide, including in East Asia. However, the lateral resolution of their long-period measurements is ∼500-750 km. Ma et al. (2018) obtained the 3D P-wave velocity structure beneath Northeast Asia and adjacent regions by performing joint inversions of local earthquakes and teleseismic events. The vertical cross-sections of P-wave velocity tomography show a ∼-1.5% low velocity structure at depth ∼300-400 km southeast of the Changbaishan volcano. Bagley et al. (2009) applied the multiple ScS reverberation method and interpret the presence of a 410-LVL oceanward of the subducting Honshu slab at an average depth of 356 km with a thickness of 50-75 km (Fig. 7). Here we use triplication waveform modeling with relatively high frequency signal up to 1-2 s and report a continuously 410-LVL that extends from the western edge of Japan Sea to the northeast China mainland (Fig. 7), covering the gap between the previously identified 410-LVL locations. Our results indicate that the velocity anomalies of the 410-LVL are about −1.5% and −2.5% for P and S, and the thickness varies between 55-80 km.

4.3. The influence of temperature on the 410-LVL

The observation of a 410-LVL has important implications for dynamic models of global mantle convection and the recycling of geochemical heterogeneities. The thermal structure of mantle is usually considered to be the first order controlling factor for anomalous mantle seismic wave speeds, such as high wave speeds associated with the subduction of cold oceanic lithosphere. Mineral physics experiments show that the variation of P-wave velocity with temperature is about -4 to -5×10^{-5} %/K (Cammarano et al., 2003). Assuming the observed 410-LVL is entirely produced by a thermal anomaly, a temperature increase of 300-375 K is required to generate a P velocity reduction of ∼1.5%. This kind of temperature anomaly will inevitably lead to the obvious depression of the 410 by 27-34 km assuming a Clapeyron slope for olivine to wadsleyite of 3 MPa/K (Ito and Takahashi, 1989). However, this predicted depression is inconsistent with our velocity models that have a small (∼15-20 km) positive elevation in the 410 depth. Likewise, receiver function analysis to the west of our study region reveals a 50 km thick 410-LVL but the 410 topography shows no obvious depression (Tauzin et al., 2017; Wang et al., 2017). Seismic tomography images near our study region reveal a low velocity anomaly at the depth of ∼300 km (Fukao and Obayashi, 2013), however, the lateral extension of this low velocity anomaly is very limited, and mostly located to the west of Changbaishan volcano, which could not account for our observed LVL. We thus conclude that purely thermal origin cannot explain the observed LVL atop the 410.

4.4. Origin of the 410-LVL: complete wetting of grain boundaries by melts

A small amount of water can affect the mineral physical properties of rocks, such as density and seismic velocity. However, even under water-saturated conditions, water can only lower the Vp and Vs up to 0.7% at ∼400 km depth (Mao and Li, 2016), which cannot explain the observed velocity anomalies of 410-LVL. Partial melting is another possibility. However, in most cases, melts do not completely wet olivine grain-boundaries (e.g., Cooper and Kohlstedt, 1982; Toramaru and Fujii, 1986) and for these data a very large amount of melt (a few %) is needed to explain a substantial (∼2% or more) velocity drop. Such a large amount of melt cannot exist in layers thicker than the compaction length (∼1 km). Consequently, partial melt is not a viable model to explain the low velocity in most cases (e.g., Karato, 2014).

We calculate the Vp/Vs ratio within the 410-LVL for the middle and southern regions, and compare them with those of the Iasp91 model (Fig. 8a). In the global Iasp91 model, the Vp/Vs ratio is high within the depth range of 350-400 km, but our regional study shows still higher values. We not only notice a significant velocity reduction atop the 410, but also a high Vp/Vs ratio, indicating a greater velocity reduction for Vs than Vp. Yoshino et al. (2007) report that hydrous melts completely wet olivine grain-boundaries under deep upper mantle conditions. If grain-boundaries are complete wetted by a melt, grain-boundaries have no resistance for shear and grain-boundary sliding will reduce the seismic wave velocities substantially (e.g., Karato, 2012), resulting a large Vp/Vs ratio.

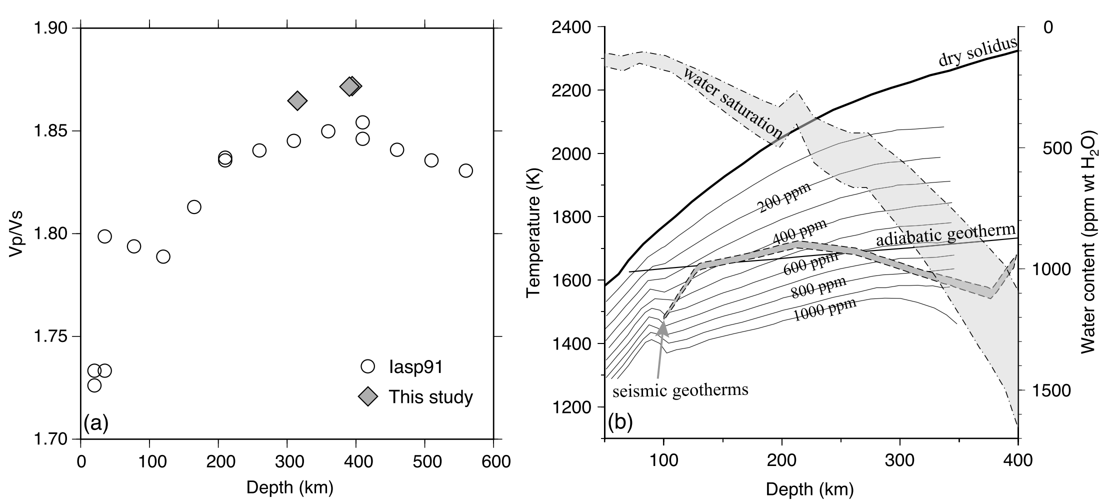

Fig. 8. (a) The Vp/Vs ratios of Iasp91 reference model (black hollow dots) and our study (gray solid diamonds). Our results clearly show high Vp/Vs ratio trend atop the 410-km discontinuity. (b) Illustration of the formation of partial melting in a peridotite dominated system. Thick line represents the dry peridotite solidus in the upper mantle, and the temperature can reach ∼2223 K at 350 km depth. Thin lines represent the influence of a small amount of water on the solidus of peridotite to partial melting (100-1000 ppm water content; Hirschmann et al., 2009). The adiabatic geotherm in the upper mantle with potential temperatures of 1530-1620 K, is far below the dry solidus (Katsura et al., 2004). The dark gray area represents the seismic geotherms deduced from P-wave velocity structures above the stagnant slab (Ichiki et al., 2006). The light gray area represents water saturation of the upper mantle, and the water storage capacity is between 750 to 1150 ppm water at 350 km depth (Férot and Bolfan-Casanova, 2012). While only ∼900-1000 ppm water can lower the dehydration melting temperature below geotherm (see discussion in section 4.4).

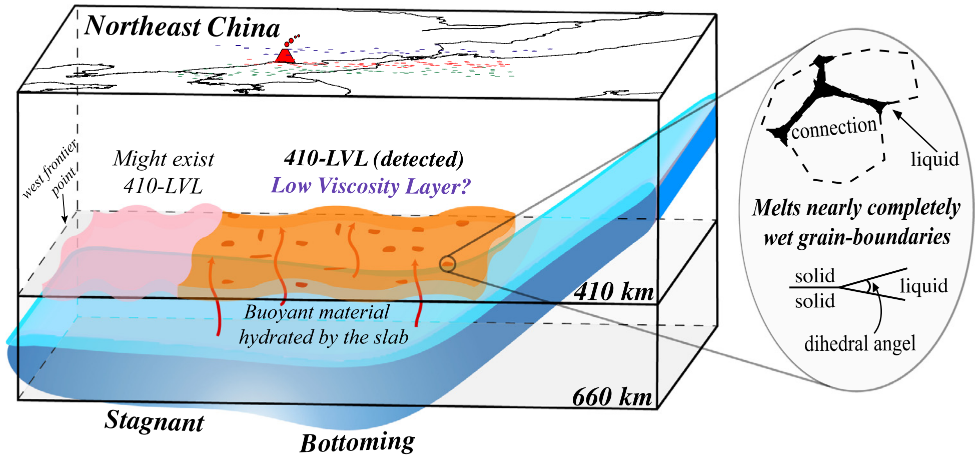

Fig. 9. Schematic map showing the 410-LVL related processes beneath northwest Pacific subduction zone. The light gray zone represents the water-bearing MTZ with 2000-4000 ppm water. The geographic map is added on the top with red symbol represents the Changbaishan volcano, and dots in different color represent the turning points of CD phase, indicating the location of the 410-LVL on earth surface. The orange irregular symbols in the middle roughly correspond to the location of 410-LVL we observed, where the grain boundaries are completely melt-wetting. This LVL might also corresponds to a low viscosity layer. The red arrows mark the buoyant material hydrated by the slab across the 410. The light pink shadow regions on the left above the 410 are the possible location of the LVL to the west. The right panel shows the morphology of liquid at the grain-boundary of crystals. If dihedral angle $<60^\circ$, liquid forms an interconnected network along the grain edge and corner, and significantly reduce seismic wave velocity (Yoshino et al., 2007; Matsukage et al., 2017). Due to the limitation of seismic stations and the method itself, we cannot resolve the west frontier point of 410-LVL. However, we expect the LVL could extend to westward further.

Beneath the northwestern Pacific subduction zone, geochemical analysis of Cenozoic intraplate basalts around Changbaishan volcano suggests intensive hydration of the MTZ which might be caused by the stagnation of the Cenozoic slab (Kuritani et al., 2011). Seismic waveform modeling shows a different P and SH velocity structure in the MTZ, which implies an estimated 2000 to 4000 ppm water there (Li et al., 2013). Recent 2D numerical simulations argue that the interaction of the hydrous MTZ and the subducting slab is responsible for the widespread intraplate volcanism and the low velocity around the subduction zone (Yang and Faccenda, 2020). All these geophysical observations and calculations indicate that the MTZ beneath east Asia is water-rich and any upwelling of material from the MTZ to the overlying upper mantle will likely promote partial melting, thereby providing a mechanism for the 410-LVL. Based on this assumption, we can estimate the lower limit of the water content required to produce partial melting at the depth of the 410. The water content needed for partial melting above the 410-km was estimated to be ~500 ppm for a typical geotherm, and a temperature of ~1800 K (Karato et al., 2006; Hirschmann et al., 2009). Ichiki et al. (2006) used the P-wave velocity model to calculate seismic geotherms in the upper mantle above the stagnant slab beneath northeast China, and the corresponding temperature at 350 km is ~1573 K (Fig. 8b). For this temperature, the necessary water content is somewhat higher, ~900-1000 ppm.

Presently there is no clear consensus regarding the formation of the 410-LVL. One model is the transition zone water filter (TZWF) hypothesis (Bercovici and Karato, 2003). Bercovici and Karato (2003) proposed that the global flow pattern in Earth's mantle is dominated by the slab-related localized downwelling current, and in most regions (except near subduction zones) a diffuse upwelling flow will occur due to the global down-going slab flux. If there is enough water in the MTZ, dehydration-induced partial melting will occur, resulting in a near global LVLs above the 410. However, the flow regime in the Pacific subduction zone is a different and the down-going convection current is dominated in this region.

In the northwest Pacific subduction zone, the horizontal deflection of the slab in the MTZ is well imaged from seismic tomography (Zhao et al., 2009; Fukao and Obayashi, 2013). The overlying mantle is relatively warmer and drier, while the stagnant slab is colder and hydrated. Warm mantle material overlying the stagnant slab would become buoyant when hydrated by the slab, and thus would likely become unstable. Eventually, the wadsleyite-dominated buoyant material in the upper MTZ will transform to an olivine-dominated assembly while crossing the 410 (Karato et al., 2006). If the water content of the ascending material exceeds the weaker water storage capacity of the upper mantle minerals, the hydrated MTZ minerals will become saturated or super-saturated. The high-water content rocks would significantly reduce the wet solidus temperature, and thus undergo partial melting at the upper boundary of the MTZ (Fig. 9). With the dihedral angle approaching to zero, the melt completely wets grain-boundaries; the grain-boundaries will lose the strength and result in the substantial reduction of seismic wave velocities.

The water content in the MTZ may be relatively high in Pacific subduction zone, and mineralogically bound water can pass efficiently through old and fast down-going subducting slabs (van Keken et al., 2011). For the northwest Pacific slab with a relatively high thermal parameter of ~5600 km, water can be brought down to at least 240 km depth due to the considerable storage of water in gabbro and peridotite lithosphere. A high-pressure experimental study on the morphology of hydrous liquid in eclogites showed that hydrous melts in eclogites are isolated and do not migrate up or down and therefore may carry water to the lowermost upper mantle and the MTZ when the slab is cold (Matsukage et al., 2017). Although quantitative dynamic and petrological models to estimate water flux in the MTZ is limited, high-temperature and high-pressure experiments showed that in the deep mantle, water can be stored in phase A, E and other nominally anhydrous minerals. The recent finding of Ice-VII inclusions in natural diamonds revealed that water-rich fluid occurs within the MTZ beneath Shandong Province, China (Tschauner et al., 2018). It is thus possible that the seismic waves sample a relatively thick part of a regional water-induced partial melting layer caused by the transport of water-rich materials (Fig. 9).

Alternatively, we cannot rule out the possibility of carbonate-induced melting within the 410-LVL. Thomson et al. (2016) found there is difficulty for deep recycling of carbonate and the resultant formation of carbonatitic melt above the MTZ. In contrast, Li et al. (2016b) found the undissolved Mg-rich carbonates can be carried into the MTZ, then rise up and begin to melt at a depth of 300-330 km. Due to the limited available studies on carbonate melts under high-temperature and high-pressure conditions, there is a great uncertainty in the estimation of the total carbon flux (Dasgupta, 2013). In combination with previous geophysical investigations of seismic wave velocity, electrical conductivity and geodynamical simulation, we favor the model for water-induced silicate melts above the 410 beneath the northwest Pacific subduction zone.

4.5. Implication in the context of subducting Pacific slab

We have demonstrated the existence of a LVL above the 410 km boundary of the MTZ beneath the northwest Pacific subduction zone (Fig. 7), and more specifically, beneath the northwestern Japan Sea region and the eastern Eurasian continental margin, a prominent "gap and blank" region where seismic instruments are very limited. The integrated picture of the distribution of the 410-LVL revealed by receiver function analysis and our regional seismic waveform modeling shows that the LVL is pervasively distributed beneath the western Pacific subduction region, covering a broad zone from ∼134°E to at least ∼ 121-123°E in lateral extent.

The estimated thickness of the 410-LVL in our study varies from 55 to 80 km, well within the previous studies that report thickness ranging from 20 to 90 km (e.g. Jasbinsek and Dueker, 2007; Tauzin et al., 2017). Given the available experimental data on melting, partial melting likely occurs in the deep upper mantle as far as the water content exceeds a critical value, for example, ∼500 ppm as suggested in previous studies (e.g., Karato et al., 2006; Hirschmann et al., 2009) or ∼900-1000 ppm as estimated for the cold regions such as the western Pacific. The compaction length in these regions, however, is very thin with a value of ∼1 km or less, and the compaction time is ∼0.01 to 1 Ma (Richter and Mckenzie, 1984; Karato, 2014); this means that after a time interval exceeding the compaction time, a large portion of melt will be accumulated in a thin layer with typical thickness of the compaction length (∼1 km or less; Karato et al., 2006). Therefore, the observed thickness of the LVL is not due to the presence of a large fraction of melt, but should be due to the complete wetting by a small amount of melt.

We infer that the 410-LVL caused by the wetting of melt would create a low viscosity layer (Fig. 9) that would mechanically decouple the upper mantle and the MTZ. A weak layer just beneath the MTZ has been proposed to play a key role in producing slab stagnation in Northern Honshu (Mao and Zhong, 2018). However, a low-viscosity-layer above the MTZ, at least locally, hasn't been invoked in previous studies. We argue that this layer might have important role in modifying the behavior of subducting slab, which need further exploration of numerical simulation.

The nature and underlying process of the observed 410-LVL is still under debate. If the mechanism related to the subducting and stagnant slab is correct, we expect that the LVL can keep stable for a long time, however, it must be formed no more than 40-60 Myr considering the age of the thickened slab trapped in the MTZ (Li et al., 2016a). The 410-LVL might be even younger than 30 Ma, as recent 3D geodynamic simulations have shown that the fast retreat of slab accompanying the open of Japan Sea play an important role in the formation of a stagnant slab (Mao and Zhong, 2018). Due to the limitation in the distribution of seismic stations, the 410-LVL reported here is confined to a near-rectangular region with a lateral range of ∼900 km, and ∼500 km in latitude, and the westernmost edge is located ∼200 km west of Changbaishan volcano. The 410-LVL may extend further westward, corresponding to the westernmost frontier point ever reached in the Cenozoic era by the subducting Pacific slab (Fig. 9), as suggested in numerical models by using high-resolution boundary element methods by Morra et al. (2016), which reveal in detail the close relationship with the clustering of diapiric upwellings with the widespread Cenozoic volcanism in east Asia.

5. Conclusion

We applied both P and S triplication waveform modeling for 5 intermediate depth earthquakes and detected a widespread low velocity layer atop the 410-km discontinuity beneath the Japan Sea, the east Eurasian continental margin and northeast China. The velocity reduction is ∼1.5% for P-waves, and ∼2.5% for SH-waves, and the thickness of the 410-LVL varies between 55-80 km. The 900 km lateral extension of the 410-LVL indicates that it is a widespread low velocity layer related to the subducting Pacific slab. We favor the interpretation that the MTZ beneath east Asia is water-rich. The buoyant and water-rich materials in the MTZ undergo partial melting while crossing the 410, completely wet grain-boundaries at the top of the MTZ, and then generate the widely distributed low velocity layer. The thickness shows that the LVL could be related to complete wetting by a small amount of melt, rather than a large fraction of melt. The LVL is inferred to also have a low viscosity, which would decouple the upper mantle and the MTZ, and thus affects the geodynamic behavior of the mantle circulation caused by the subducting slab.

CRediT authorship contribution statement

Guangjie Han: Conceptualization, Formal analysis, Investigation, Methodology, Software, Validation, Visualization, Writing - original draft, Writing - review & editing. **Juan Li:** Conceptualization, Data curation, Funding acquisition, Project administration, Resources, Supervision, Writing - review & editing. **Guangrui Guo:** Investigation, Visualization, Writing - review & editing. **Walter D. Mooney:** Writing - review & editing. **Shun-ichiro Karato:** Funding acquisition, Writing - review & editing. **David A. Yuen:** Funding acquisition, Writing - review & editing.

Declaration of competing interest

The authors declare that they have no known competing financial interests or personal relationships that could have appeared to influence the work reported in this paper.

Acknowledgement

This research is supported by the Strategic Priority Research Program (B) of Chinese Academy of Sciences (Grant: XDB18010302), NSFC (J. Li, Grant: 41774065, 41322026) and the Key Research Program of the Institute of Geology & Geophysics, CAS, grant IGGCAS-201904; David A. Yuen acknowledges partial support from the US Department of Energy Grant DE-SC0019759 and the National Science Foundation (NSF) Grant EAR-1918126, Shun-ichiro Karato acknowledges support from NSF-CSEDI program (Grant: EAR-1764271) and Walter D. Mooney received support from the USGS Earthquake Hazards Program. We thank the Editor and the two anonymous reviewers for comments which improved the quality of the manuscript significantly. We thank the Data Management Centre of China National Seismic Network at Institute of Geophysics, the Seismic Array Laboratory at Institute of Geology and Geophysics and IRIS DMS, for providing seismic data. We thank the Supercomputing Laboratory, IGGCAS for the computing resource. Sac2000, Tau-P and GMT software are used in basic data processing and plotting of most figures.

Appendix A. Supplementary material

Supplementary material related to this article can be found online at https://doi.org/10.1016/j.epsl.2020.116642.

References

Bagley, B., Courtier, A.M., Revenaugh, J., 2009. Melting in the deep upper mantle oceanward of the Honshu slab. Phys. Earth Planet. Inter. 175 (3–4), 137–144. https://doi.org/10.1016/j.pepi.2009.03.007.

Bercovici, D., Karato, S., 2003. Whole-mantle convection and the transition-zone water filter. Nature 425 (6953), 39–44. https://doi.org/10.1038/nature01918.

Cammarano, F., Goes, S., Vacher, P., Giardini, D., 2003. Inferring upper-mantle temperatures from seismic velocities. Phys. Earth Planet. Inter. 138 (3–4), 197–222. https://doi.org/10.1016/s0031-9201(03)00156-0.

Cooper, R.F., Kohlstedt, D.L., 1982. Interfacial energies in the olivine-basalt system. In: Manghnani, M.H., Akimoto, S.-I. (Eds.), High-Pressure Research in Geophysics. Academic Press Inc, New York, pp. 217–228.

Dasgupta, R., 2013. Ingassing, storage, and outgassing of terrestrial carbon through geologic time. Rev. Mineral. Geochem. 75, 183–229. https://doi.org/10.2138/rmg.2013.75.7.

Férot, A., Bolfan-Casanova, N., 2012. Water storage capacity in olivine and pyroxene to 14 GPa: implications for the water content of the Earth's upper mantle and nature of seismic discontinuities. Earth Planet. Sci. Lett. 349–350, 218–230. https://doi.org/10.1016/j.epsl.2012.06.022.

Fukao, Y., Obayashi, M., 2013. Subducted slabs stagnant above, penetrating through, and trapped below the 660 km discontinuity. J. Geophys. Res., Solid Earth 118 (11), 5920–5938. https://doi.org/10.1002/2013jb010466.

Hirschmann, M.M., Tenner, T., Aubaud, C., Withers, A.C., 2009. Dehydration melting of nominally anhydrous mantle: the primacy of partitioning. Phys. Earth Planet. Inter. 176 (1–2), 54–68. https://doi.org/10.1016/j.pepi.2009.04.001.

Ichiki, M., Baba, K., Obayashi, M., Utada, H., 2006. Water content and geotherm in the upper mantle above the stagnant slab: interpretation of electrical conductivity and seismic P-wave velocity models. Phys. Earth Planet. Inter. 155 (1–2), 1–15. https://doi.org/10.1016/j.pepi.2005.09.010.

Ito, E., Takahashi, E., 1989. Postspinel transformations in the system Mg_2SiO_4-Fe_2SiO_4 and some geophysical implications. J. Geophys. Res. B, Solid Earth Planets 94 (B8), 10637–10646. https://doi.org/10.1029/JB094iB08p10637.

Jasbinsek, J., Dueker, K., 2007. Ubiquitous low-velocity layer atop the 410-km discontinuity in the northern Rocky Mountains. Geochem. Geophys. Geosyst. 8, Q10004. https://doi.org/10.1029/2007gc001661.

Karato, S.I., 2014. Does partial melting explain geophysical anomalies? Phys. Earth Planet. Inter. 228, 300–306. https://doi.org/10.1016/j.pepi.2013.08.006.

Karato, S.I., 2012. On the origin of the asthenosphere. Earth Planet. Sci. Lett. 321, 95–103. https://doi.org/10.1016/j.epsl.2012.01.001.

Karato, S.I., Bercovici, D., Leahy, G., Richard, G., Jing, Z., 2006. The transition-zone water filter model for global material circulation: where do we stand. In: Jacobsen, S.D., Lee, S.V.D. (Eds.), Earth's Deep Water Cycle. American Geophysical Union, Washington, D.C., pp. 289–313.

Katsura, T., Yamada, H., Nishikawa, O., Song, M.S., Kubo, A., Shinmei, T., Yokoshi, S., Aizawa, Y., Yoshino, T., Walter, M.J., Ito, E., Funakoshi, K., 2004. Olivine-wadsleyite transition in the system (Mg, $Fe)_2SiO_4$. J. Geophys. Res., Solid Earth 109 (B2). https://doi.org/10.1029/2003jb002438.

Kuritani, T., Ohtani, E., Kimura, J.I., 2011. Intensive hydration of the mantle transition zone beneath China caused by ancient slab stagnation. Nat. Geosci. 4 (10), 713–716. https://doi.org/10.1038/ngeo1250.

Li, D., Helmberger, D., Clayton, R.W., Sun, D., 2014. Global synthetic seismograms using a 2-D finite-difference method. Geophys. J. Int. 197 (2), 1166–1183. https://doi.org/10.1093/gji/ggu050.

Li, J., Tosi, N., Maierová, P., Yuen, D.A., 2016a. Evidence from caustic waveform modeling for long slab thickening above the 660-km discontinuity under Northeast Asia: dynamic implications. In: King, S.D., Lee, S.-M., Morra, G., Stein, S., Yuen, D.A. (Eds.), Subduction Dynamics: from Mantle Flow to Mega Disasters, first ed. American Geophysical Union and John Wiley & Sons, Inc., Washington, D.C., pp. 5–18.

Li, J., Wang, X., Wang, X., Yuen, D.A., 2013. P and SH velocity structure in the upper mantle beneath Northeast China: evidence for a stagnant slab in hydrous mantle transition zone. Earth Planet. Sci. Lett. 367, 71–81. https://doi.org/10.1016/j.epsl.2013.02.026.

Li, S., Yang, W., Ke, S., Meng, X., Tian, H., Xu, L., He, Y., Huang, J., Wang, X.-C., Xia, Q., Sun, W., Yang, X., Ren, Z.-Y., Wei, H., Liu, Y., Meng, F., Yan, J., 2016b. Deep carbon cycles constrained by a large-scale mantle Mg isotope anomaly in eastern China. Nat. Sci. Rev. 4 (1), 111–120. https://doi.org/10.1093/nsr/nww070.

Liu, Z., Park, J., Karato, S.I., 2016. Seismological detection of low-velocity anomalies surrounding the mantle transition zone in Japan subduction zone. Geophys. Res. Lett. 43 (6), 2480–2487. https://doi.org/10.1002/2015gl067097.

Ma, J., Tian, Y., Liu, C., Zhao, D., Feng, X., Zhu, H., 2018. P-wave tomography of Northeast Asia: constraints on the western Pacific plate subduction and mantle dynamics. Phys. Earth Planet. Inter. 274, 105–126. https://doi.org/10.1016/j.pepi.2017.11.003.

Mao, W., Zhong, S.J., 2018. Slab stagnation due to a reduced viscosity layer beneath the mantle transition zone. Nat. Geosci. 11 (11), 876–881. https://doi.org/10.1038/s41561-018-0225-2.

Mao, Z., Li, X., 2016. Effect of hydration on the elasticity of mantle minerals and its geophysical implications. Sci. China Earth Sci. 59 (5), 873–888. https://doi.org/10.1007/s11430-016-5277-9.

Matsukage, K.N., Hashimoto, M., Nishihara, Y., 2017. Morphological stability of hydrous liquid droplets at grain boundaries of eclogite minerals in the deep upper mantle. J. Mineral. Petrol. Sci. 112 (6), 346–358. https://doi.org/10.2465/jmps.170309.

Morra, G.F., Yuen, D.A., Lee, S.M., Zhang, S., 2016. Source of the Cenozoic Volcanism in Central Asia. In: Morra, G.F., Yuen, D.A., King, S.D., Lee, S.M., Stein, S. (Eds.), Subduction Dynamics: from Mantle Flow to Mega Disasters, first ed. American Geophysical Union and John Wiley & Sons, Inc., Washington, D.C., pp. 97–113.

Niu, F., Li, J., 2011. Component azimuths of the CEArray stations estimated from P-wave particle motion. Earthq. Sci. 24 (1), 3–13. https://doi.org/10.1007/s11589-011-0764-8.

Revenaugh, J., Sipkin, S.A., 1994. Seismic evidence for silicate melt atop the 410 km mantle discontinuity. Nature 369 (6480), 474–476. https://doi.org/10.1038/369474a0.

Richter, F.M., Mckenzie, D., 1984. Dynamical models for melt segregation from a deformable matrix. J. Geol. 92 (6), 729–740. https://doi.org/10.1086/628908.

Tang, Y., Obayashi, M., Niu, F., Grand, S.P., Chen, Y.J., Kawakatsu, H., Tanaka, S., Ning, J., Ni, J.F., 2014. Changbaishan volcanism in northeast China linked to subduction-induced mantle upwelling. Nat. Geosci. 7 (6), 470–475. https://doi.org/10.1038/ngeo2166.

Tauzin, B., Debayle, E., Wittlinger, G., 2010. Seismic evidence for a global low-velocity layer within the Earth's upper mantle. Nat. Geosci. 3 (10), 718–721. https://doi.org/10.1038/Ngeo969.

Tauzin, B., Kim, S., Kennett, B.L.N., 2017. Pervasive seismic low-velocity zones within stagnant plates in the mantle transition zone: thermal or compositional origin? Earth Planet. Sci. Lett. 477, 1–13. https://doi.org/10.1016/j.epsl.2017.08.006.

Thomson, A.R., Walter, M.J., Kohn, S.C., Brooker, R.A., 2016. Slab melting as a barrier to deep carbon subduction. Nature 529 (7584), 76–79. https://doi.org/10.1038/nature16174.

Tian, Y., Zhu, H., Zhao, D., Liu, C., Feng, X., Liu, T., Ma, J., 2016. Mantle transition zone structure beneath the Changbai volcano: Insight into deep slab dehydration and hot upwelling near the 410 km discontinuity. J. Geophys. Res., Solid Earth 121 (8), 5794–5808. https://doi.org/10.1002/2016jb012959.

Toramaru, A., Fujii, N., 1986. Connectivity of melt phase in a partially molten peridotite. J. Geophys. Res., Solid Earth 91 (B9), 9239–9252. https://doi.org/10.1029/JB091iB09p09239.

Tschauner, O., Huang, S., Greenberg, E., Prakapenka, V.B., Ma, C., Rossman, G.R., Shen, A.H., Zhang, D., Newville, M., Lanzirotti, A., Tait, K., 2018. Ice-VII inclusions in diamonds: evidence for aqueous fluid in Earth's deep mantle. Science 359 (6380), 1136–1139. https://doi.org/10.1126/science.aao3030.

van Keken, P.E., Hacker, B.R., Syracuse, E.M., Abers, G.A., 2011. Subduction factory: 4. Depth-dependent flux of H_2O from subducting slabs worldwide. J. Geophys. Res. 116, B01401. https://doi.org/10.1029/2010jb007922.

Vinnik, L., 2002. Subcratonic low-velocity layer and flood basalts. Geophys. Res. Lett. 29 (4). https://doi.org/10.1029/2001gl014064.

Wang, R.J., 1999. A simple orthonormalization method for stable and efficient computation of Green's functions. Bull. Seismol. Soc. Am. 89 (3), 733–741.

Wang, T., Revenaugh, J., Song, X.D., 2014. Two-dimensional/three-dimensional waveform modeling of subducting slab and transition zone beneath Northeast Asia. J. Geophys. Res., Solid Earth 119 (6), 4766–4786. https://doi.org/10.1002/2014jb011058.

Wang, X., Chen, Q.F., Li, J., Wei, S.J., 2016. Seismic sensor misorientation measurement using P-wave particle motion: an application to the NECsaids Array. Seismol. Res. Lett. 87 (4), 901–911. https://doi.org/10.1785/0220160005.

Wang, X., Li, J., Chen, Q.F., 2017. Topography of the 410 km and 660 km discontinuities beneath the Japan Sea and adjacent regions by analysis of multiple-ScS waves. J. Geophys. Res., Solid Earth 122 (2), 1264–1283. https://doi.org/10.1002/2016jb013357.

Wang, Y., Wen, L., Weidner, D., He, Y., 2006. SHvelocity and compositional models near the 660-km discontinuity beneath South America and northeast Asia. J. Geophys. Res. 111 (B7). https://doi.org/10.1029/2005jb003849.

Wei, S.S., Shearer, P.M., 2017. A sporadic low-velocity layer atop the 410 km discontinuity beneath the Pacific Ocean. J. Geophys. Res., Solid Earth 122 (7), 5144–5159. https://doi.org/10.1002/2017jb014100.

Yang, J., Faccenda, M., 2020. Intraplate volcanism originating from upwelling hydrous mantle transition zone. Nature 579 (7797), 88–91. https://doi.org/10.1038/s41586-020-2045-y.

Ye, L.L., Li, J., Tseng, T.L., Yao, Z.X., 2011. A stagnant slab in a water-bearing mantle transition zone beneath northeast China: implications from regional SH waveform modelling. Geophys. J. Int. 186 (2), 706–710. https://doi.org/10.1111/j.1365-246X.2011.05063.x.

Yoshino, T., Yu, N., Karato, S., 2007. Complete wetting of olivine grain boundaries by a hydrous melt near the mantle transition zone. Earth Planet. Sci. Lett. 256 (3–4), 466–472. https://doi.org/10.1016/j.epsl.2007.02.002.

Zhao, D., Ohtani, E., 2009. Deep slab subduction and dehydration and their geodynamic consequences: evidence from seismology and mineral physics. Gondwana Res. 16 (3–4), 401–413. https://doi.org/10.1016/j.gr.2009.01.005.

Zhao, D., Tian, Y., Lei, J., Liu, L., Zheng, S., 2009. Seismic image and origin of the Changbai intraplate volcano in East Asia: role of big mantle wedge above the stagnant Pacific slab. Phys. Earth Planet. Inter. 173 (3–4), 197–206. https://doi.org/10.1016/j.pepi.2008.11.009.

Zheng, X.F., Yao, Z.X., Liang, J.H., Zheng, J., 2010. The role played and opportunities provided by IGP DMC of China national seismic network in wenchuan earthquake disaster relief and researches. Bull. Seismol. Soc. Am. 100 (5B), 2866–2872. https://doi.org/10.1785/0120090257.